

# International Symposium on Thermal Problems in Space-Based Systems

*presented at*

THE WINTER ANNUAL MEETING OF  
THE AMERICAN SOCIETY OF MECHANICAL ENGINEERS  
BOSTON, MASSACHUSETTS  
DECEMBER 13-18, 1987

*sponsored by*

THE COMMITTEE ON THEORY AND FUNDAMENTAL RESEARCH,  
THE HEAT TRANSFER DIVISION, ASME

*edited by*

FLAVIO DOBRAN  
NEW YORK UNIVERSITY

MURRAY IMBER  
POLYTECHNIC UNIVERSITY

Library of Congress Catalog Card Number 87-73097

Statement from By-Laws: The Society shall not be responsible for statements or opinions advanced in papers . . . or printed in its publications (7.1.3)

Any paper from this volume may be reproduced without written permission as long as the authors and publisher are acknowledged.

Copyright ©1987 by  
THE AMERICAN SOCIETY OF MECHANICAL ENGINEERS  
All Rights Reserved  
Printed in U.S.A.

## FOREWORD

The diversity of fluid mechanics and heat transfer problems pertaining to the space-based systems is attested by the present volume of papers. The practical relevance of the results of these papers ranges from the design of the space station, space instruments, space vehicles and space power conversion systems to the problems involved in the space manufacturing. One of the great challenges of the future is to perfect the skills that will not only establish the man's presence in space on a more permanent basis, but also to enable him to utilize the unique features of this environment. Clearly, the technical problems are enormous and the current symposium volume is an effort to bring together the research efforts pertaining to the heat transfer in space-based systems. The range of problems considered in the papers includes: super heat pipe design considerations and transient testing; transient conduction effects in target plates due to the high power laser irradiation and the low temperature radiometer design considerations; theoretical and experimental investigations of forced convection condensation with suction at the wall and gas-liquid flow pattern identification under the microgravity conditions of space; design of boiling heat transfer and flow separation experiments for space; the use of general purpose fluid mechanics and heat transfer programs for the design of space station and other space vehicles; liquid metal magnetohydrodynamic two-phase flow power conversion system analysis; crystal manufacturing in a microgravity environment; and analysis of heat transfer problems associated with the space plane and fluid behavior under a rapid depressurization to the vacuum of space.

The editors wish to express their appreciation to all the authors who submitted abstracts and papers for the symposium. We also wish to acknowledge the help of reviewers whose efforts have improved the quality of the papers. Our special thanks are extended to the Innovative Science and Technology Directorate of the Strategic Defense Initiative Organization which provided partial support for widely advertising the purpose and scope of this international symposium.

Flavio Dobran  
Murray Imber

## REVIEWERS

O. A. Arnas	H. R. Jacobs
A. A. Bishop	D. W. Jannitell
H. Branover	A. S. Jordan
L. C. Chow	W. E. Langlois
S. W. Churchill	M. Morduchow
G. T. Colwell	G. P. Peterson
F. Dobran	W. M. Rohsenow
M. A. Ebadian	R. P. Scaringe
C. P. Grigoropoulos	R. A. Seban
T. J. Hanratty	S. Subrammanian
P. G. Hill	R. L. Webb
M. Imber	J. Weisman

## CONTENTS

Super Heat Pipe Design Considerations for Applications to Space-Based Systems <i>F. Dobran</i> . . . . .	1
Two-Dimensional Thermal Conduction Effects in High Power CW Laser Target Plates <i>M. A. Shadday, Jr. and J. R. Couick</i> . . . . .	13
Applicability of the Flow-Net Program to Solution of Space Station Fluid Dynamics Problems <i>J. Navickas and W. C. Rivard</i> . . . . .	19
Low Gravity Venting of R-11, A Model <i>A. F. Romero-Lopez and H. Merte, Jr.</i> . . . . .	25
Experimental Investigation of Low Gravity Two-Phase Flow Behavior <i>G. L. Yoder, Jr., E. D. Brewer, J. E. Hardy, W. B. Jatko, and R. N. Nodine</i> . . . . .	31
Transient Conduction-Radiation Analysis of an Absolute Active Cavity Radiometer Using Finite Elements <i>J. R. Mahan, F. Kowsary, N. Tira, and B. D. Gardiner</i> . . . . .	39
Some Thermal Problems of Space Power LMMHD Converters <i>F. Werkoff, P. Lecocq, S. Chaudourne, A. Alemany, and R. Laborde</i> . . . . .	49
Response of a Double Wall Artery Heat Pipe to Pulsed Heat Loads <i>R. Ponnappan, M. L. Ramalingam, J. E. Beam, and E. T. Mahefkey</i> . . . . .	55
The Marangoni Convection on a Germanium Float Zone <i>M. Z. Saghir</i> . . . . .	63
Forced Condensation in a Tube With Suction at the Wall for Microgravitational Applications <i>A. Faghri and L. C. Chow</i> . . . . .	71
Natural Convection in a Cylinder Caused by Gravitational Interferences: A Three-Dimensional Numerical Calculation <i>S. Schneider, T. Heiss, and J. Straub</i> . . . . .	77
Gas Liquid Flow at Microgravity Conditions: Flow Patterns and Their Transitions <i>A. E. Dukler, J. A. Fabre, J. B. McQuillen, and R. Vernon</i> . . . . .	85
Ascent and Reentry Heat Rejection Concepts for Hermes Space Plane <i>B. J. G. Leidinge and H. R. Muller</i> . . . . .	99
Conjugating Binary Solutions for Spacecraft Thermal Control <i>P. G. Grodzka and J. W. Owen</i> . . . . .	109
Preliminary Investigation of Advanced Heat Pump Augmented Spacecraft Heat Rejection Systems <i>R. P. Scaringe</i> . . . . .	119
Application of Two-Phase Thermal Transport Systems to Space Platforms <i>C. E. Braun, J. E. Fredley, V. J. Gilberti, and K. Hartshorn</i> . . . . .	125
Orbital Replaceable Unit-Cold Plate Dry Thermal Interface Concept and Test Measurements <i>D. Nikanpour, H. K. Sill, and H. Kreeb</i> . . . . .	135



## SUPER HEAT PIPE DESIGN CONSIDERATIONS FOR APPLICATIONS TO SPACE-BASED SYSTEMS

F. Dobran  
New York University  
Applied Science Department  
New York, New York

### ABSTRACT

The design of space-based systems using heat pipes should strive towards reliability and optimum heat transfer without exceeding the heat transfer operating limits. The heat pipe operating limits can be suppressed and some of them eliminated through a judicious design or optimization involving the heat transfer surface and vapor and liquid flow channels. In the paper the current high heat transfer performance heat pipes are discussed and a super heat pipe defined for the purpose of providing the design goals. A consideration of the optimal vapor flow in high temperature heat pipes shows that the axial heat transport capacity depends on the working fluid, vapor flow area, on the method of vapor introduction into the main core flow of the evaporator or withdrawal from the condenser, and on the lengths of the evaporator, adiabatic and condenser regions. A parametric study is also presented and methods identified to suppress the axial heat transport limits. The design considerations for optimal boiling and wicking limits in heat pipes should involve an operation close to the nucleate boiling fluxes on the evaporator surfaces made of reentrant grooves or sintered metal powder structures, with the liquid flowing from the condenser to the evaporator through separate liquid channels.

### NOMENCLATURE

a - Defined by Eq.(35)  
A - Flow cross-sectional area  
b - Defined by Eq.(27)  
c - Speed of sound defined by Eq.(2)  
C - Defined by Eq.(34)  
C<sub>p</sub> - Specific heat at constant pressure  
d<sub>a</sub> - Average grain size of the porous matrix  
D<sup>D</sup> - Hydraulic diameter  
f - Friction coefficient defined by Eq.(12)  
g - Body force per unit mass  
h - Enthalpy  
h<sub>g</sub> - Enthalpy of evaporation  
H<sub>g</sub> - Energy term defined by Eq.(9)  
k - Ratio of specific heats  
K - Permeability defined by Eq.(38)

L - Heat pipe length  
L<sub>eff</sub> - Heat pipe effective length for the heat transport,  $0.5(L_e + L_c) + L_a$   
m - Coefficient in Eq.(18)<sup>a</sup>  
M - Mach number, V/c  
n - Coefficient in Eq.(18)  
P - Pressure  
P<sub>er</sub> - Perimeter  
q<sub>er</sub> - Heat transfer rate per unit length  
q<sub>s</sub> - Sonic limit heat transfer rate per unit length  
Q<sub>s</sub> - Heat transfer rate  
R - Gas constant  
Re - Reynolds number,  $wD(1-y_i)/\mu A$   
T - Temperature  
V - Velocity  
V<sub>i</sub>' - Axial component of the injection velocity, Fig. 5  
w<sub>i</sub>' - Mass flow rate  
x - Axial coordinate along the heat pipe  
y<sub>i</sub>' - V<sub>i</sub>'/V  
ε<sub>i</sub>' - Porosity  
μ - Viscosity  
ρ - Density  
τ - Shear stress

### Subscripts

a - Adiabatic region of heat pipe  
c - Condenser region of heat pipe  
e - Evaporator region of heat pipe  
eff - Effective  
i - Vapor injection or withdrawal  
l - Pertains to the liquid phase  
o - Stagnation condition at the evaporator inlet  
p - Porous metal surface  
s - Sonic condition  
v - Vapor  
w - Wall

### 1. OVERVIEW OF HEAT PIPE APPLICATIONS FOR SPACE-BASED SYSTEMS

Heat pipes are very useful heat transfer devices for the design of space-based systems. They are used for the thermal control of satellites and other spacecrafts, to separate heat sources from heat sinks

as in the envisioned space power systems of the future, for the heat flux transformation, etc. The specific application determines the heat pipe's operating temperature, working fluid, and material of its construction, whereas the nature of the application determines the heat pipe's detailed design characteristics such as the internal liquid and vapor flow geometry and external shape. The heat pipe application temperatures may range from the liquid helium temperature at a few degrees Kelvin (for maintaining low temperatures of infrared detectors) to a thousand or more degrees as in the cooling of rocket combustion chambers and envisioned space nuclear reactor cores.

Dobran [1] recently reviewed the heat pipe technology for terrestrial and space systems applications and found that most of the current heat pipe research and development efforts pertain to the applications to space-based systems. The United States is currently designing a space station and considering various options for large space power systems and future manned and unmanned missions [2-5]. The thermal control of space station as illustrated in Fig. 1 [4] will require the control of various modules. Its power requirement may start at about 75 KW and expand to about 300 KW which will require the dissipation of large quantities of heat into space through the thermal radiators. These radiators are envisioned to be constructed from the modular heat pipe units and assembled in space into the Space Constructible Radiators (SCR) [6,7]. For the thermal control of the space station's modules, the ammonia heat pipes are preferable due to their high performance level from -50 to 100 C and compatibility with the lightweight aluminum material. The dissipation of thermal energy into space by the heat rejection system of the photovoltaic and solar dynamic power modules of the space station can be 125 KW for a net generation capacity of 25 KW and an efficiency of conversion of 20%. To reduce the radiator area the heat pipes used in these radiators should operate at higher temperatures than those of the radiators for the thermal control of space modules discussed above. At higher temperatures the heat pipe's working fluid methanol becomes more desirable than ammonia, but then it must be used with a heat pipe material made of stainless steel owing to the incompatibility of this fluid with aluminum.

The initial large capacity (about 300 KW) space power system is envisioned to be of a nuclear type [2] with a very compact design and its core operating at about 1000 C [8,9]. Because of this requirement, Merrigan et al. [10] discuss the typical heat transfer conditions of a space nuclear reactor as: (1) 100-200 W/cm<sup>2</sup> radial power density, (2) 10 KW/cm<sup>2</sup> axial power density, (3) long adiabatic sections to provide separation between the nuclear core and conversion system, and (4) an operation close to the material limits. These researchers also note that for the cooling of a space nuclear reactor high temperature heat pipes with the working fluids potassium, sodium and lithium offer several favorable characteristics such as self-regulation and start-up, decay heat removal after the reactor shut-down, and a high reliability. The lithium heat pipe discussed in Reference 10 was designed with the above performance requirements in view.

The above heat pipe design requirements for applications in the space-based nuclear reactors place a limit on the current heat pipe technology, and the heat pipes operating under these heat transfer rates

may be viewed as super heat pipes. Through research and by the judicious optimization of the heat pipe design parameters it is possible to design heat pipes beyond the current limits. The objectives of this paper are: (1) to discuss the heat pipes' heat transfer operating limits and present current high performance heat pipe designs where some of these limits have been eliminated or suppressed, and (2) to present some considerations towards the design of super heat pipes for optimal vapor flow and boiling and wicking heat transfer limits.

## 2. HEAT PIPE OPERATING LIMITS

The basic heat pipe configuration is illustrated in Fig. 2. It consists of a container such as a pipe whose interior wall is lined with a porous wick structure saturated with a working fluid. Heat transfer in the evaporator region of the heat pipe causes the liquid in the wick to evaporate and flow into the condenser zone where it is condensed. The return of liquid from the condenser to the evaporator occurs due to the capillary forces in the wick which create a surface tension pressure difference required to overcome the vapor and liquid pressure drops as well as that due to gravitation or other externally imposed body forces.

The thermohydrodynamic flow aspects in a heat pipe determine, for a given geometry pipe and working fluid, its heat transport limits. The depletion of liquid on the surface of the evaporator produces a dryout condition and may yield a burnout of the heat transfer surface due to the large surface temperature of the material wall. This burnout heat transfer or boiling limit may also be reached if the amount of liquid in a heat pipe is small or the capillary wick ceases to supply properly the liquid from the condenser to the evaporator. The capillary wick will function properly if the liquid wets the surface of the porous wick structure because the liquid will then be readily drawn into and saturate the wick pores by the surface tension force. Each porous wick structure is endowed with a capillary heat flux limit where an effective liquid supply (pumping) from the condenser to the evaporator ceases. The difference in the shape of the effective interface between the evaporator and condenser creates an effective pressure gradient for liquid flow which increases with small wick pores but at the expense of the simultaneous increase in the liquid flow resistance.

At high axial heat fluxes and in long heat pipes the countercurrent flow of liquid and vapor produces an instability of the liquid-vapor interface yielding the liquid droplets entrainment from the liquid in the wick into the vapor in the core or an entrainment heat flux limit where any further increase in the vapor flow by heat addition, for example, cannot sustain anymore an increase in the liquid condensate flow. The decrease of the liquid flow into the evaporator may, in this situation, produce a burnout of the evaporator surface and violent fluid oscillations if means exist (gravity, for example) for the accumulated liquid in the condenser to suddenly return into the evaporator.

When the design of a heat pipe overcomes the liquid flow limitations, the vapor flow can produce sonic and viscous flow limiting operations. The sonic or choked flow heat transfer limit is produced under the control of the inertia forces in the vapor. Heat addition or mass injection in the evaporator accelerates the vapor and can produce choking at the

evaporator exit where the Mach number reaches unity. For this situation to occur, the downstream condenser temperature must be sufficiently low and its further decrease will not produce an increase in the heat flux in the evaporator. Figure 3 illustrates the experimental data of Kemme [11] taken in a sodium heat pipe with no adiabatic region. Curve A in this figure corresponds to the subsonic flow in the evaporator and condenser, whereas the curve B corresponds to the sonic flow condition at the evaporator exit. Curves C and D correspond to the situation of a supersonic flow in the condenser region close to the evaporator and vapor flow deceleration through shocks. The mass withdrawal in the condenser has the tendency to produce large nonuniformities in the flow properties in the radial direction and may yield flow reversals. For this reason, the shock regions in the condenser are poorly defined (see Fig. 3). Near the working fluid's freezing point the vapor density is low and a heat pipe is more prone to choking than at higher temperatures. Fluids such as sodium and lithium have low vapor densities and are, therefore, more influenced by the sonic heat flux limit than other high vapor density fluids.

When the inertia and viscous forces of the vapor are of the same order of magnitude, the choking occurs at the condenser inlet, since the subsonic flow in the adiabatic region with friction can only produce a Mach number increase [12,13]. With negligible inertia forces, however, choking does not occur [14]. The heat flux increases steadily with decreasing pressure at the evaporator exit and becomes limited by a zero vapor pressure. This heat transfer limit is called the viscous limit.

The operation of a heat pipe close to the working fluid's thermodynamic critical point can be very erratic with small changes in the heat flux or temperature boundary conditions at the evaporator and condenser surfaces owing to the large gradients of thermodynamic properties close to this point [15]. The gravitational effects or artificially created gravity in space due to the centrifugal, electrostatic or electromagnetic forces may produce limiting heat pipe operations too, since these forces may impede the liquid and vapor flow. High density fluids, such as water, methanol, mercury and cesium, are sensitive to the gravitational effects, whereas the low density fluids such as sodium and lithium are much less sensitive and may not severely impede the heat pipe operation in an adverse gravitational or force field.

The noncondensable gas in a heat pipe can be used to accurately control the temperature or device of a space-based system. These Variable Conductance Heat Pipes (VCHP) are often used in satellites and with the noncondensable gas of a lower molecular weight than that of the working fluid's vapor [16] in order to keep the gas in the condenser region. However, the distribution of the noncondensable gas in the condenser depends on the diffusion, convective mixing and buoyancy between the gas and vapor [17,18]. For low-to-moderate heat loads in VCHP's, the condensation front may occur in the near-to-mid section of the condenser with the heat pipe heat transfer performance depending on the heat losses from adiabatic and condenser regions. In these situations the role of heat losses must be recognized in the analysis as shown by Bobco [16].

Of particular importance in the design of space-based systems using heat pipes is the recognition and the understanding of the heat pipe's transient

behavior, owing to the fact that a heat pipe during the power-up, transient loading and shut-down must pass through the transient states. The transient heat pipe response is dictated by the thermal capacity of the heat pipe shell, capillary structure and working fluid, on the liquid and vapor flow characteristics, and on the heat flux distribution in the evaporator and condenser. Colwell and Chang [15] studied the transient response of a F-11 heat pipe and classified the transient heat pipe operation into four modes: (1) the heat transfer is modest and the heat pipe smoothly and easily (in seconds) accommodates the changes on the heat transfer surfaces with the capillaries being fully wetted; (2) the heat transfer is such that a portion of the capillary structure in the evaporator dries and large temperature variations occur, but the heat pipe nevertheless reaches a steady state operation after a certain time; (3) the heat pipe fails completely as a result of the excessive heat transfer rates; and (4) a start-up from the thermodynamic supercritical state (as in the cryogenic heat pipes) which requires at first bringing the working fluid into a two-phase mixture region, or a start-up from the frozen fluid state where the working fluid must first be melted and vaporized to start the normal heat pipe operation. Heat pipes with high vapor density fluids when started from room temperature attain a uniform start-up rate because of the establishment of fast working fluid circulation. When the vapor densities of working fluids are low and the temperature of the medium surrounding the heat pipe is also low, such that the molecular free path of the vapor exceeds the vapor channel diameter, the start-up becomes frontal [19] and the heat transfer close to the evaporator end will be primarily determined by convection and close to the condenser end by conduction, with the two separating zones possessing a frontal region. A more detailed description of the recent heat pipe transient research efforts is described by Dobran [1] and the reader is referred to this reference for further details and references.

### 3. HIGH PERFORMANCE HEAT PIPE DESIGN CONSIDERATIONS

#### 3.1 Definition of a Super Heat Pipe

A super heat pipe can be defined as a heat pipe that can transfer an optimum heat transfer rate. This optimum heat transfer rate is determined:

- (1) By the application (temperature range and control requirements, heat transfer rate, heat flux transformation, environmental conditions, space or geometric constraints in a space-based system, etc).
- (2) By the working fluid (safety considerations, compatibility with the heat pipe material, etc.)
- (3) By the heat pipe's external and internal geometry (external evaporator and condenser characteristics; characteristics of the wick or internal porous surface structures in evaporator and condenser such as porosity and particle size distribution; shapes of the liquid, if any, and vapor flow channels; design of capillaries to redistribute the liquid in the evaporator for efficient evaporation and in the condenser for the efficient vapor condensation; vapor injection characteristics in the evaporator such as predominantly parallel-to-the-main-flow direction or perpendicular to it; the degree of intentionally created supersaturation of the vapor; etc.).

A super heat pipe operates, therefore, close to its heat transfer limits, most of which have been

eliminated or suppressed through a judicious design optimization.

### 3.2 Current High Performance Heat Pipe Designs

Table 1 summarizes the current high heat transfer performance heat pipe designs and test results [1]. All of these heat pipes have been designed to eliminate or suppress one or more of the heat transfer limits discussed above. As will be seen in the following sections, however, there is much room left for further performance improvements.

The monogroove heat pipe shown in Table 1 and Fig. 4a was developed by Grumman [20]. It contains separate axial channels for the liquid and vapor flow. The slot separating the two channels serves the purpose of creating a high capillary pressure difference, whereas the circumferential grooves in the vapor channel serve the purpose of distributing the liquid flowing through the slot. The heat pipe dimensions given in the table were optimized for heat transfer with ammonia and applications to thermal radiators of the space station. The two-channel design provides a considerable separation between the liquid and vapor flows and for the most part eliminates the flooding or countercurrent flow limiting operation. The liquid viscous pressure drop is also minimal because the liquid flows through a channel without obstructions as opposed to the flow in a wick in conventional heat pipe designs (see Fig. 2). The circumferential grooves in the vapor channel not only provide an effective liquid distribution, but also maximize the heat transfer area for the evaporation of liquid. The heat transfer to and from the heat pipe occurs through the radiator fin attached to the vapor channel (Fig. 4a) and the liquid boiling in the liquid channel is suppressed.

The presence of a noncondensable gas or vapor in the liquid channel of a monogroove heat pipe may lead to the heat pipe depriming and loss of performance. The tapered artery heat pipe shown in Fig. 4b is designed to suppress this problem because of the provision for automatic bubble or gas venting from the liquid channel by means of the tapered shape of the channel [21]. The trapezoidally axially grooved heat pipe in Table 1 was designed to provide self priming capability in 1-g and minimum susceptibility to the boiling heat flux limit [22]. The dual slot heat pipe [23] shown in the table consists of a flat baffle that separates the vapor channel from the liquid channel. The circumferential grooves, machined on the inside of the circular tube, provide for the capillary wicking action to transport the working fluid in the evaporator from the liquid channel to the vapor channel by means of the surface tension force. In the condenser section the circumferential grooves provide a path for the condensate to flow from the vapor to the liquid channel. The meniscus between the two slots formed where the baffle touches the inner wall of the tube sustains the pumping pressure differential.

The double wall artery heat pipe [24] illustrated in Table 1 and Fig. 4c consists of a composite wick geometry where the liquid and vapor flow paths have been separated and high radial heat transfer rates achieved through the careful design of the liquid arteries close to the pipe wall. This heat pipe consists of a concentric tube arrangement with the inner tube externally grooved for the liquid transport and slotted to allow for the vapor venting. The evaporator section also includes a screen between the inner surface of the outer pipe and outer grooved

surface of the inner slotted pipe for the purpose of maximizing heat transfer and self-priming capability.

Merrigan et al. [10] developed a dual pair artery liquid metal heat pipe as shown in Fig. 4d for the operation with lithium at about 1200 C. As shown in Table 1, this heat pipe achieved an axial power density of 19 KW/cm<sup>2</sup> and radial heat fluxes of 150 W/cm<sup>2</sup>, with more than 100 hours of continuous operation without the degradation of performance. Other high temperature liquid metal heat pipes are discussed in [1,25]. These include the niobium-zirconium heat pipes for use with sodium and lithium from 1000 to 1200 C and nickel-iron heat pipes for use with sodium or potassium from 400 to 800 C. Some of the wick structures developed at Thermacore [25] include: sintered powder metal tunnel arteries (Fig. 4e), and sintered axial grooves and flexible arteries [26]. The sintered metal wick structures provide a superior heat transfer performance to other wick designs due to the direct bonding of wick to the heat transfer surface which reduces the thermal resistance to heat transfer. The molybdenum/lithium heat pipe in Fig. 4e operated at 1900 C transferring 6 KW against gravity at an axial power density of 21.6 KW/cm<sup>2</sup> and at a radial power density of 150 W/cm<sup>2</sup> - apparently the highest demonstrated heat pipe performance level [25].

### 3.3 Heat Pipe Design Considerations for Optimal Vapor Flow

The vapor flow thermohydrodynamics in a heat pipe determines the sonic heat transfer limit. In this section further considerations will be given to this important limit by discussing methods for its suppression. The heat transfer limitations associated with the boiling and wicking limits will be discussed in the subsequent sections.

For the purpose of determining the first order effects of vapor flow in a heat pipe, use will be made of the one-dimensional and steady state compressible flow analysis. Figure 5 illustrates the vapor core region and defines the flow variables and a control volume that will be used to derive a set of equations for the analysis. For simplicity, and with a good approximation, the vapor will be assumed to obey a perfect gas equation of state, i.e.

$$P = \rho RT \quad (1)$$

The speed of sound is thus

$$c = (kRT)^{1/2} \quad (2)$$

and the Mach number is defined as

$$M = V/c \quad (3)$$

The conservation of mass at an axial position x of the heat pipe is

$$w = \rho VA \quad (4)$$

$$dw = \frac{q}{h_{fg}} dx \quad (5)$$

where dw is positive for the injected mass in the evaporator and negative for the withdrawn mass in the condenser, and q is the heat flux rate per unit length of evaporator (positive) or condenser (negative) and represents the heat transfer capability of the working fluid.



Applying the first law of thermodynamics to the control volume in Fig. 5 yields

$$dQ = dh + d\left(\frac{V^2}{2}\right) + \left[h - h_i + \frac{1}{2}(V^2 - V_i^2)\right] \frac{dw}{w} \quad (6)$$

where the potential energy terms have been neglected. For an ideal gas, the enthalpy is given as

$$dh = Cp dT \quad (7)$$

so that when substituted into Eq.(6) and use made of Eq.(2) we obtain

$$\frac{dQ+dH}{CpT} = \frac{dT}{T} + \frac{k-1}{2} M^2 \frac{dV^2}{V^2} \quad (8)$$

where

$$dH = - \frac{h - h_i + \frac{1}{2}(V^2 - V_i^2)}{CpT} \frac{dw}{w} \quad (9)$$

represents the effect of injection or nonequilibrium between the liquid-vapor interface and mean vapor core parameters.

The momentum equation gives

$$-AdP - \tau_w P_{er} dx + g\rho A dx = d(wV) - Vy_i dw \quad (10)$$

where

$$y_i = \frac{V'_i}{V} \quad (11)$$

represents the directional effect of the injected or withdrawn mass (see Fig. 5). Using the definition of the friction factor and hydraulic diameter, i.e.

$$f = \frac{\tau_w}{\frac{1}{2}\rho V^2}, \quad D = \frac{4A}{P_{er}} \quad (12)$$

the momentum Eq.(10) can be written as follows

$$\frac{dP}{P} + \frac{kM^2}{2} \frac{dV^2}{V^2} + \frac{kM^2}{2} 4f \frac{dx}{D} - M^2 gk \frac{dx}{V^2} + kM^2(1-y_i) \frac{dw}{w} = 0 \quad (13)$$

where use is made of Eqs.(1) and (3).

From the definition of stagnation temperature, speed of sound, and Mach number we have

$$T_o = T + \frac{V^2}{2Cp} = T\left(1 + \frac{k-1}{2}M^2\right) \quad (14)$$

so that Eq.(8) can also be written as

$$\frac{dQ+dH}{CpT} = \left(1 + \frac{k-1}{2}M^2\right) \frac{dT_o}{T_o} \quad (15)$$

Equations (1)-(4) and (13)-(15) give 7 equations with 11 variables P,  $\rho$ , T, c, M, V, T<sub>o</sub>, w, A, (dQ+dH)/CpT, and

$$4f \frac{dx}{D} - 2g \frac{dx}{V^2} - 2y_i \frac{dw}{w}$$

where four may be chosen as independent. Choosing the

last four in this list as independent variables it is then possible to manipulate the above equations and solve for the remaining seven dependent variables. For example, the solutions for the Mach number and pressure distributions are

$$\frac{dM^2}{M} = \frac{1+kM^2}{1-M^2} \frac{dQ+dH}{CpT} + \frac{kM^2(1+\frac{k-1}{2}M^2)}{1-M^2} \left[4f \frac{dx}{D} - 2g \frac{dx}{V^2} - 2y_i \frac{dw}{w}\right] + \frac{2(1+kM^2)(1+\frac{k-1}{2}M^2)}{1-M^2} \frac{dw}{w} - \frac{2(1+\frac{k-1}{2}M^2)}{1-M^2} \frac{dA}{A} \quad (16)$$

$$\frac{dP}{P} = - \frac{kM^2}{1-M^2} \frac{dQ+dH}{CpT} - \frac{kM^2(1+(k-1)M^2)}{2(1-M^2)} \left[4f \frac{dx}{D} - 2g \frac{dx}{V^2} - 2y_i \frac{dw}{w}\right] - \frac{2kM^2(1+\frac{k-1}{2}M^2)}{1-M^2} \frac{dw}{w} + \frac{kM^2}{1-M^2} \frac{dA}{A} \quad (17)$$

Equations (16) and (17) are similar to the results of Ref. 12 (chapter 8) where the influence coefficients multiply the independent variables. In these equations dw can be replaced by the evaporation or condensation heat flux (Eq.(5)) and the friction coefficient by

$$f = mRe^{-n} \quad (18)$$

$$Re = \frac{\rho(V-V'_i)D}{\mu} = \frac{wD(1-y_i)}{\mu A} \quad (19)$$

where the coefficients m and n depend on whether the flow is laminar or turbulent and with or without the mass injection or withdrawal. For the vapor flow in the adiabatic region of a heat pipe,  $y_i=0$  and m and n may be taken as

$$m = 16, \quad n = 1; \text{ laminar flow (Re} < 2000) \quad (20)$$

$$m = 0.079, \quad n = 0.25; \text{ turbulent flow (Re} \geq 2000)$$

The velocity profile of a laminar incompressible flow in the evaporator has a cosine rather than a parabolic distribution [14,27] with

$$m = 2\pi^2, \quad n = 1 \quad (21)$$

In the condenser with high heat transfer rates it is dangerous to use the above analysis and laminar flow expressions for the friction factor owing to the possibility of flow reversals (secondary flow) in this region as discussed previously. High heat fluxes produce high radial Reynolds numbers of the vapor in the evaporator and condenser and yield a turbulent flow in cylindrical condensers even if the axial Reynolds number is below 2000 [28].

Equations (16) and (17) can be used to study the effects of the external heat transfer, Q, vapor injection and suction,  $y_i$ , the degree of vapor nonequilibrium,  $h-h_i$ , gravity, g, and vapor flow area, A, on the limiting heat transfer rates in heat pipes. Thus Levy [29] neglected the frictional effects, area change, gravitational effect, and assumed that  $dQ+dH=0$  and  $y_i=0$ . From Eq. (16) it then follows that

$$\frac{dM^2}{M^2} = \frac{2(1+kM^2)(1+\frac{k-1}{2}M^2)}{1-M^2} \frac{dw}{w} \quad (22)$$

and upon combining with Eq.(5) it can be integrated from  $M(x=0)=0$  and  $w(x=0)=0$  to  $M(x=L_e)=1$  and  $w(x=L_e)=qL_e/h_{lv}$  to obtain an expression for the commonly utilized sonic heat flux limit  $q_s$ , i.e.

$$q_s L_e = \frac{\rho_o c_o h_{lv} A}{(2(k+1))^{1/2}} \quad (23)$$

where  $\rho_o$  and  $c_o$  are the (stagnation) density and speed of sound at the evaporator inlet. When an account is also taken of the frictional effects in the above analysis and choking assumed at the condenser inlet, it was found numerically [13] that the computed heat transfer limits agree better with data than the predictions using Eq.(23).

To investigate the more general solution of Eq.(16) we may take  $dQ+dH=0$ ,  $g=0$ , and assume that the flow is laminar. Thus

(i) Evaporator or Condenser Regions

$$\frac{1-M^2}{M^2(2+(k-1)M^2)} dM^2 = (1+aM^2) \frac{dw}{w} - \frac{dA}{A} \quad (24)$$

where

$$a = k(1-y_1) + \frac{2mk\mu Ah_{lv}}{(1-y_1)D^2 q} \quad (25)$$

(ii) Adiabatic Region

$$\frac{1-M^2}{M^2(2+(k-1)M^2)} dM^2 = bM^2 dx - \frac{dA}{A} \quad (26)$$

where

$$b = \frac{2mk\mu Ah_{lv}}{D^2 q L_e} \quad (27)$$

Moreover, by taking  $A=\text{constant}$  and  $y_1=\text{constant}$ , the solutions of Eqs.(24) and (26) between any two regions 1 and 2 are given by

(i) Evaporator and Condenser Regions

$$\frac{M_2}{M_1} \left( \frac{1+\frac{k-1}{2}M_1^2}{1+\frac{k-1}{2}M_2^2} \right)^{1/2} \left( \frac{1+\frac{k-1}{2}M_2^2}{1+\frac{k-1}{2}M_1^2} \right)^{1/2} \frac{1+aM_1^2}{1+aM_2^2} \frac{1+a}{1+2a-k} = \frac{w_2}{w_1} \quad (28)$$

(ii) Adiabatic Region

$$\frac{1}{2} \left( \frac{1}{M_1^2} - \frac{1}{M_2^2} \right) + \ln \left( \frac{M_1^2}{M_2^2} \frac{1+\frac{k-1}{2}M_2^2}{1+\frac{k-1}{2}M_1^2} \right)^{(k+1)/4} = b(x_2-x_1) \quad (29)$$

In particular, the solution represented by Eq.(23) is a special case of the solution expressed by Eq.(28). This may be proved by taking in the latter equation  $y_1=0$ ,  $\mu=0$  ( $a=k$ ),  $w_1=\rho_1 c_1 M_1 A$ ,  $M_1(x=0)=0$ ,  $M_2(x=L_e)=1$ , and  $w_2=qL_e/h_{lv}$ .

The more useful forms of Eqs.(28) and (29) are obtained by solving these equations for the maximum heat transfer rate  $q$  which occurs when the flow chokes at the exit of the adiabatic region of a heat pipe.

Setting in Eq.(28)  $w_1=\rho_1 c_1 M_1 A$ ,  $M_1(x=0)=0$ ,  $w_2=qL_e/h_{lv}$  and  $M_2=M_e$  (exit of the evaporator), and in Eq.(29)  $M_1(x=L_e)=M_e$ ,  $M_2(x=L_e+L_a)=1$  and  $x_2-x_1=L_a$ , we obtain the following results

$$\frac{qL_e}{h_{lv} \rho_o c_o A} = \frac{M_e}{(1+\frac{k-1}{2}M_e^2)^{1/2}} \left( \frac{1+\frac{k-1}{2}M_e^2}{1+aM_e^2} \right)^{1/2} \frac{1+a}{1+2a-k} \quad (30)$$

$$\frac{1}{2} \left( \frac{1}{M_e^2} - 1 \right) + \ln \left( \frac{k+1}{2} \frac{M_e^2}{1+\frac{k-1}{2}M_e^2} \right)^{(k+1)/4} = bL_a \quad (31)$$

and after normalizing by the sonic heat flux limit  $q_s$  (Eq.(23)), it follows that

$$\frac{q}{q_s} = M_e \left( \frac{2(k+1)}{1+\frac{k-1}{2}M_e^2} \right)^{1/2} \left( \frac{1+\frac{k-1}{2}M_e^2}{1+aM_e^2} \right)^{1/2} \frac{1+a}{1+2a-k} \quad (32)$$

$$\frac{1}{2} \left( \frac{1}{M_e^2} - 1 \right) + \ln \left( \frac{k+1}{2} \frac{M_e^2}{1+\frac{k-1}{2}M_e^2} \right)^{(k+1)/4} = Ck \left( \frac{L_a}{L_e} \right) \left( \frac{q}{q_s} \right) \quad (33)$$

$$C = 2m \left( \frac{\mu}{\rho_o c_o D} \right) \frac{L_e}{D} (2(k+1))^{1/2} \quad (34)$$

$$a = k \left[ (1-y_1) + \frac{C}{(1-y_1)} \left( \frac{q}{q_s} \right) \right] \quad (35)$$

In particular, when  $L=0$  and  $M=1$  (choking at the evaporator exit), Eq.(32) is reduced to the form

$$\frac{q}{q_s} = 2 \left( \frac{k+1}{2(1+a)} \right)^{1/2} \frac{1+a}{1+2a-k} \quad (36)$$

Equations (32) and (33) can now be solved for  $q/q_s$  in terms of the independent parameters  $C, k, L_a/L_e$  and  $y_1$ , or since  $\mu, \rho_o, c_o$  and  $k$  can be evaluated at the saturation temperature at the evaporator inlet, the independent variables may also be taken as  $T_{sat}, D, L_a/D, L_a/L_e$  and  $y_1$ .

Figures 6 and 7 illustrate the predicted heat transfer rates with the sonic flow at the evaporator and adiabatic section exits, respectively, and a comparison with the sodium, potassium, and cesium data [11,13,30,31]. The analytical results in these figures were generated by assuming that  $y_1=0$  (normal-to-the-main-flow vapor injection in the evaporator) and using the perfect gas equation of state for the calculation of density and speed of sound at the saturation temperature at the evaporator inlet. As can be seen from these figures, the inclusion of frictional effects into the model produces a superior comparison of analysis with data and reduces axial heat transport capacities of heat pipes. At high temperatures, some sodium data [30,31] show a deviation from the sonic heat transfer limit behavior and may be associated with attainment of the wicking heat flux limits in heat pipes as discussed earlier. At lower temperatures, the heat pipe performance becomes sensitive on the frictional effects, and the axial heat transfer capacity can be considerably reduced as illustrated in

Fig. 7 which shows a good comparison of analysis with data with a finite length of the adiabatic region.

The effects of the vapor diameter  $D$ , evaporator length to diameter ratio,  $L/D$ , and adiabatic length to the evaporator length ratio,  $L_a/L_e$ , on the sonic heat flux limits for lithium, sodium, and cesium is illustrated in Fig. 8. At constant  $D$ , an increase of the evaporator and adiabatic lengths has the effect of reducing heat pipe's axial heat transport capacity; this reduction is considerable for long heat pipes and at lower temperatures where the frictional effects become more important. With the temperature and evaporator and adiabatic lengths fixed, a heat pipe with a larger vapor flow area can transport larger axial heat fluxes for all fluids in Fig. 8. The axial heat transport capacities of  $Li$  are also more sensitive to the frictional effects (and, therefore, on  $L_a$  and  $L_e$ ) than those of  $Na$ ,  $K$  and  $Cs$ .

Figure 9 shows the effect of the non-normal-to-the-main-flow vapor injection in the evaporator ( $y_i > 0$ ). Large values of  $y_i$  are seen to produce a considerable decrease of the sonic heat flux limits for  $Li$  and  $Na$  at lower temperatures and a slight increase beyond the frictionless sonic heat flux limit at very high temperatures. The physical explanation of these results is that at lower temperatures the frictional effects are important, whereas at high temperatures the inertial effects dominate and require higher axial heat fluxes for  $y_i > 0$  than for  $y_i = 0$  for the attainment of a sonic limit (see Eq.(24)).

Equation (24) also shows that an area increase for the vapor flow in the evaporator and adiabatic regions of a heat pipe can produce larger sonic heat flux limits than in a uniform area pipe. This implies that heat pipes with long evaporator and adiabatic sections may require nonuniform cross-sectional areas for vapor flow ( $dA/dx > 0$ ) in order to compensate for the reduction of sonic heat flux limits brought about by the frictional effects. For applications to space-based systems, a super heat pipe system may be envisioned with a heat source supplying heat to variable cross-sectional areas of the evaporators of heat pipes which in turn transfer this heat to the power conversion system which may be removed by a considerable distance from the power source.

### 3.4 Heat Pipe Design Considerations for Optimal Boiling Limits

Very large heat transfer rates in heat pipes are limited by the boiling heat flux limit. This limit can be suppressed, but not eliminated, through the judicious design of the evaporator heat transfer surfaces. As discussed in section 3.2, the current high performance heat pipes are designed with sintered metal powder surfaces where porous metal structures are bonded to the inside walls of evaporators.

High performance heat transfer surfaces for applications to heat pipes are characterized by the nucleate boiling heat fluxes. These fluxes may be achieved through: (1) "structured" surfaces having reentrant groove-type cavities, and (2) porous coatings. Webb [32,33] surveyed the evolution of both types of these surfaces for the nucleate boiling heat transfer performance and came with the following conclusions:

(i) The cavity geometry is important in two ways: the mouth diameter determines the superheat needed to

initiate boiling, and its shape determines its stability once boiling has begun.

(ii) The cavity should be reentrant with its internal shape not being important. The liquid superheat required to maintain a vapor nucleus is inversely proportional to its radius of curvature which in a reentrant cavity can be negative in the presence of a subcooled liquid.

(iii) The manufacturing of discrete wall cavities is difficult and the commercially feasible concepts should strive towards the production of high-area density nucleation sites.

(iv) The reentrant cavities can be manufactured through etching, electroplating, piercing the three-dimensional cover sheets, attaching wire or screen promoters, use of nonwetting coatings, porous metal or fiber coatings, production of integral roughness (nucleation sites interconnected below the surface with tunnels and reentrant configurations), etc.

The sintered metal powder and fiber surfaces not only provide large nucleate boiling heat fluxes but also high capillary pressure rises due to small pore sizes. The most significant characteristics of a porous matrix are the average pore size radius and porosity [32]. Larger pore sizes can be used with high surface tension and high thermal conductivity fluids, whereas small pore sizes should be used with low surface tension and low thermal conductivity fluids such as fluorocarbon refrigerants. The heat transfer performance of a porous surface appears to be optimal with coating thicknesses in the neighborhood of four particle diameters, at least for copper spherical particles from 100 to 500  $\mu m$  with R-113 boiling [33].

The key factors attributed to the high heat transport performance of porous and reentrant grooved structures are: (1) a pore or reentrant cavity within a critical size range, (2) interconnected cavities, and (3) nucleation sites of a reentrant type. The interconnection of cavities provides for the activation of adjacent cavities during boiling, and a porous structure allows for large vaporization rates on presumably very thin liquid films within the subsurface structure. It is not possible, however, for a stable vapor bubble or boiling to exist within a cavity whose surfaces are wetted by a thin liquid film, since the vapor and liquid can only coexist with a finite liquid contact angle, or the cavity will be filled with liquid. For this reason, a "static" boiling model of O'Neil [34], which assumes the existence of a stable film surrounding the bubble, is difficult to justify, although it gives reasonably accurate values of the maximum boiling fluxes [32]. The determination of boiling heat flux limits in porous structures should involve a "dynamic" model which accounts for two-phase flow in the capillary channels.

### 3.5 Heat Pipe Design Consideration for Optimal Wicking Heat Flux Limit

The wicking heat flux limits in heat pipes are associated with the liquid pumping capacities in the wick structures. Using the Darcy's law for the laminar and one-dimensional flow in porous media, the pressure change of liquid from the condenser exit ( $x=L_e+L_a+L_c$ ) to the evaporator inlet ( $x=0$ ) (see Fig. 2) is

$$\Delta P_{\lambda} = \rho g L \cos \phi + \frac{\mu_{\lambda} W_{\lambda}}{\rho_{\lambda} A_p K} L_{\text{eff}} \quad (37)$$

where  $A_p$  is the total flow cross-sectional of the porous medium,  $g \cos \phi$  is the component of gravity in the direction of flow,  $L_{eff}$  is the effective length for heat transfer, and  $K_{eff}$  is the permeability of the medium which may be modeled by a constitutive equation due to Carman [35], i.e.

$$K = \frac{\epsilon^2 d_p^2}{180(1-\epsilon)^2} \quad (38)$$

From the above equations it may be seen than small size particles and porosities of a porous material yield small permeabilities and require large pressure drops for liquid to flow through the porous structures. Since the capillary pressure rise (which is inversely proportional to the average pore diameter) must exceed the pressure losses in the liquid, in the vapor, and those due to gravity for a reliable heat pipe operation, it is clear that the porous material may limit the heat pipe's heat transfer capacity. The maximum liquid pumping occurs when the liquid wets the evaporator wick perfectly and the meniscus radius is equal to the radius of the average pore size. A heat transfer rate to the evaporator causing the liquid to retreat into the wick and evaporator to dry out produces the boiling heat flux limiting operation as discussed above.

To avoid the wicking limit in heat pipes, high performance heat pipes are designed with the liquid flowing from condenser to evaporator in separate channels and not through a porous structure (see Table 1 and Fig. 4), for then the liquid pressure drop is reduced permitting larger liquid flow rates which can transfer larger heat fluxes. In long heat pipes the pressure drop in the liquid channels must be reduced through additional design considerations, such as by distributing the liquid to flow in parallel channels or using the environmental characteristics of a space-based system (artificial gravity and solar energy for pumping, etc.).

#### 4. SUMMARY AND CONCLUSIONS

The current designs of space-based systems use heat pipes for variety of tasks, ranging from the thermal control of satellites and space station to the removal of heat in the future space nuclear reactor operating at high temperatures. These applications require a reliable and efficient heat pipe design over a large range of the system and environmental conditions. For these reasons, the heat pipe design has strived toward the development of super heat pipes which transfer optimum heat transfer rates without exceeding the heat transfer operating limits. Many of these limits may be suppressed and some may be eliminated through a judicious optimization of heat pipe geometry and selection of working fluids.

In the paper a definition of a super heat pipe is given and some considerations given for the design of high temperature heat pipes where the sonic flow and frictional effects can severely limit the axial heat transport capacities. The heat pipe design considerations for the optimal boiling and wicking limits were also considered. The porous metal structures and reentrant cavities on the evaporator heat transfer surface can support very large nucleate boiling fluxes and large capillary pressure rises allowing large mass flow rates and heat transfers, provided that the liquid is made to flow from the

condenser to the evaporator through separate liquid channels which minimize pressure drops.

#### REFERENCES

- [1] Dobran, F., "Heat Pipe Research and Development in the Americas," Proceedings of 6th International Heat Pipe Conference, May 25-28, 1987, Grenoble, France.
- [2] Vanlandingham, E.E., "The NASA Space Power Technology Program," Intersociety Energy Conversion Engineering Conference, Vol. 3, 1986, pp.1405-1410.
- [3] Barthelemy, R.R., Massie, L.D., and Borger, W.U., "Military Space Power Systems Technology for the Twenty-First Century," Intersociety Energy Conversion Engineering Conference, Vol. 3, 1986, pp.1401-1404.
- [4] Desanctis, C., Priest, C., and Wood, W., "Space Station Overview," AIAA 25th Aerospace Sciences Meeting, Paper AIAA-86-0315, January 12-15, 1987, Reno, Nevada.
- [5] Sadunas, J.A., and Lehtinen, A., "Thermal Management Systems Options for the High Power Space Platforms," AIAA 20th Thermophysics Conference, Paper AIAA-85-1047, June 19-21, 1985, Williamsburg, Virginia.
- [6] Oren, J.A., and Cox, R.L., "Thermal Management for Large Space Platforms," J. Spacecraft and Rockets, Vol. 19, 1982, pp.278-283.
- [7] Baer, T., "Space Station Thermal Control," Mechanical Engineering, December 1984, pp.22-33.
- [8] Merrigan, M.A., Keddy, E.S., Sena, J.T., and Elder, M.G., "Heat Pipe Technology Development for High Temperature Space Radiator Applications," Intersociety Energy Conversion Engineering Conference, Vol. 1, 1984, pp.592-597.
- [9] Merrigan, M.A., "Heat Pipe Design for Space Power Heat Rejection Applications," Intersociety Energy Conversion Engineering Conference, Vol. 3, 1986, pp.1993-1998.
- [10] Merrigan, M.A., Martinez, E.H., Keddy, E.S., Runyan, J.E., and Kemme, J.E., "Performance Demonstration of a High Power Space Reactor Heat Pipe Design," Intersociety Energy Conversion Engineering Conference, Vol. 4, 1983, pp.1874-1879.
- [11] Kemme, J.E., "Ultimate Heat Pipe Performance," IEEE Transactions on Electron Devices, Vol. ED-16, 1969, pp.717-723.
- [12] Shapiro, A.H., Compressible Fluid Flow, Vol. 1, Ronald, New York, 1953.
- [13] Levy, E.K., and Chou, S.F., "The Sonic Limit in Sodium Heat Pipes," J. Heat Transfer, May 1973, pp.218-223.
- [14] Busse, C.A., "Theory of the Ultimate Heat Transfer Limit of Cylindrical Heat Pipes," Int. J. Heat Mass Transfer, Vol. 16, 1973, pp.169-186.
- [15] Colwell, G.T., and Chang, W.S., "Measurements of the Transient Behavior of a Capillary Structure Under Heavy Thermal Loading," Int. J. Heat Mass Transfer, Vol. 27, 1984, pp.541-551.
- [16] Bobco, R.P., "Variable Conductance Heat Pipes: A



First-Order Model," J. Thermophysics, Vol. 1, 1987, pp.35-42.

[17] Hijikata, K., Chen, S.J., and Tien, C.L., "Noncondensable Gas Effect on Condensation in a Two-Phase Closed Thermosyphon," Int. J. Heat Mass Transfer, Vol. 27, 1984, pp.1319-1325.

[18] Peterson, P.F., and Tien, C.L., "A Miniature Wet Bulb Technique for Measuring Gas Concentrations in Condensing or Evaporating Systems," to appear in Experimental Heat Transfer, Vol. 1, 1987, Personal communication with C.L. Tien.

[19] Beam, J.E., "Transient Heat Pipe Analysis," AIAA 20th Thermophysics Conference, Paper AIAA-85-0936, June 19-21, 1985, Williamsburg, Virginia.

[20] Alario, J., Haslett, R., and Cosson, R., "the Monogroove High Performance Heat Pipe," Progress in Astronautics and Aeronautics, Vol. 83, 1982, pp.305-324.

[21] Holmes, H.R., and Feild, A.R., "The Gas-Tolerant High Capacity Tapered Artery Heat Pipe," AIAA/ASME 4th Joint Thermophysics and Heat Transfer Conference, Paper AIAA-86-1343, June 2-4, 1986, Boston, Massachusetts.

[22] Richter, R.F.G., and Brennan, "Development of an Advanced Trapezoidal Axially Grooved (ATAG) Heat Pipe," AIAA/ASME 4th Joint Thermophysics and Heat Transfer Conference, Paper AIAA-86-1342, June 2-4, 1986, Boston, Massachusetts.

[23] Carlson, A.W., and Gustafson, E., "Heat Pipe Radiator Technology for Space Power Systems," AIAA/ASME 4th Joint Thermophysics and Heat Transfer Conference, Paper AIAA-86-1300, June 2-4, 1986, Boston, Massachusetts.

[24] Ponnappan, R., Beam, J.E., and Mahefkey, E.T., "Improved Double-Wall Artery High-Capacity Heat Pipe," J. Spacecraft and Rockets, Vol. 22, 1985, pp.592-597.

[25] Ernst, D.W. and Eastman, G.Y., "High Temperature Heat Pipe Technology at Thermacore," AIAA 20th Thermophysics Conference, Paper AIAA-85-0981, June 19-21, 1985, Williamsburg, Virginia.

[26] Shaubach, R.M., and Gernert, N.J., "High Performance Flexible Heat Pipes," AIAA 20th Thermophysics Conference, Paper AIAA-85-1085, June 19-21, 1985, Williamsburg, Virginia.

[27] Bankston, C.A., and Smith, H.J., "Incompressible Laminar Vapor Flow in Cylindrical Heat Pipes," ASME Paper 71-WA/HT-15, 1971.

[28] Quaille, J.P., and Levy, E.K., "Laminar Flow in a Porous Tube With Suction," J. Heat Transfer, February 1975, pp.66-71.

[29] Levy, E.K., "Theoretical Investigation of Heat Pipes Operating at Low Vapor Pressures," J. Engineering for Industry, November 1968, pp.547-522.

[30] Kemme, J.E., "Heat Pipe Capability Experiments," IEEE Thermionic Conversion Conference, November 3-4, 1966, Houston, Texas, pp.159-168.

[31] Dzakowic, G., Tang, Y., and Arcella, F., "Experimental Study of Vapor Velocity Limit in a Sodium Heat Pipe," ASME Paper 69-HT-21, 1969.

[32] Webb, R.L., "The Evolution of Enhanced Surface Geometries for Nucleate Boiling," Heat Transfer Engineering, Vol. 2, 1981, pp.46-69.

[33] Webb, R.L., "Nucleate Boiling on Porous Coated Surfaces," Heat Transfer Engineering, Vol. 4, 1983, 71-82.

[34] O'Neill, P.S., Gottzman, C.F., and Terbot, J.W., "Novel Heat Exchanger Increases Cascade Cycle Efficiency for Natural Gas Liquefaction," in Advances in Cryogenic Engineering, ed. K.D. Timmerhaus, Plenum, New York, 1972, pp.420-437.

[35] Carman, P.C., "Fluid Flow Through a Granular Bed," Trans. of the Institute of Chemical Engineers, London, Vol. 15, 1937, pp.150-156.

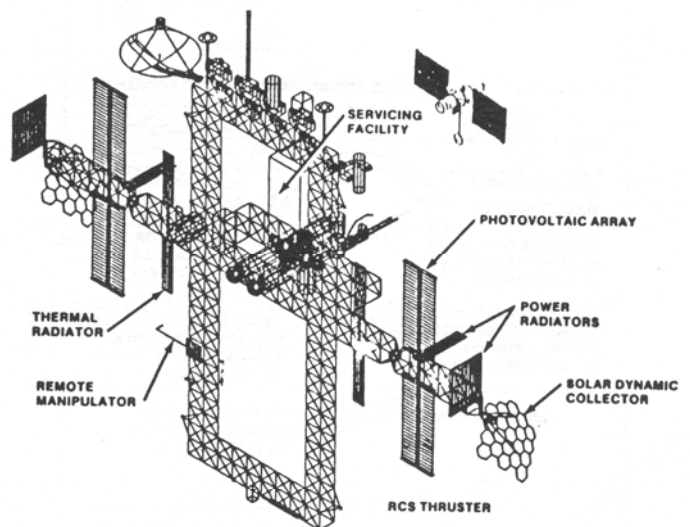


Fig. 1 NASA's space station configuration  
Copyright © AIAA; reprinted with permission

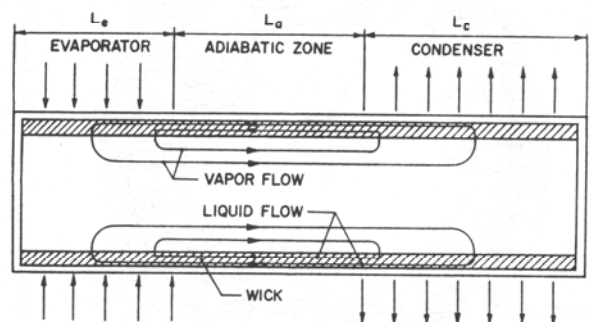


Fig. 2 Basic heat pipe configuration

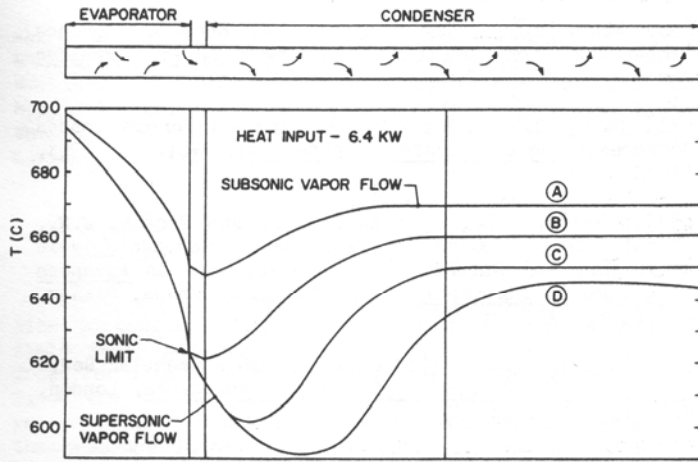


Fig. 3 Temperature distribution in a sodium heat pipe, Kemme (1969)

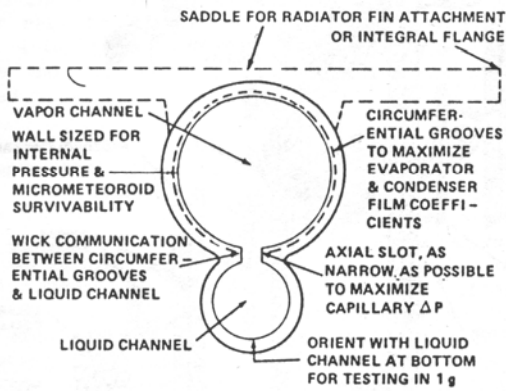


Fig. 4a Monogroove heat pipe

Copyright © AIAA; reprinted with permission

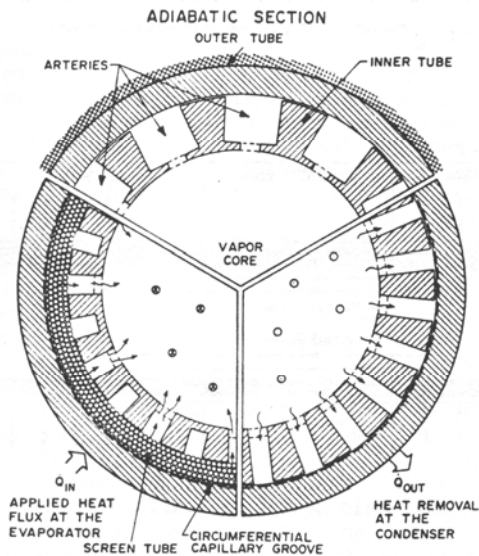


Fig. 4c Double-wall artery heat pipe

Copyright © AIAA; reprinted with permission

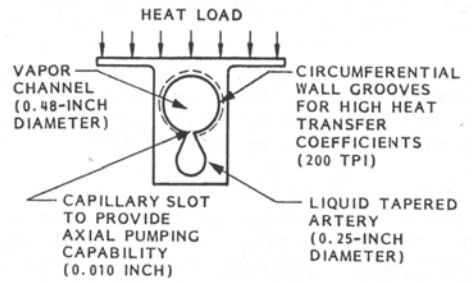


Fig. 4b Tapered artery heat pipe

Copyright © AIAA; reprinted with permission

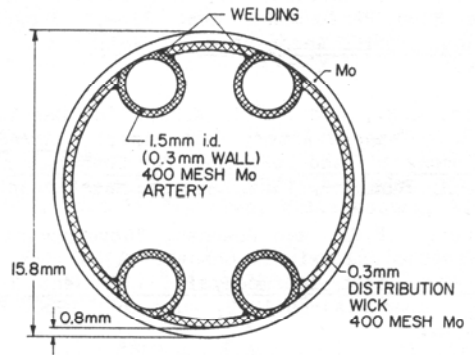


Fig. 4d Dual-pair artery heat pipe

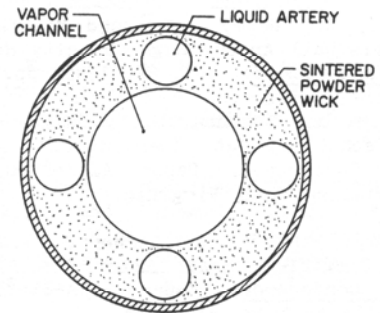


Fig. 4e Sintered-tunnel artery heat pipe

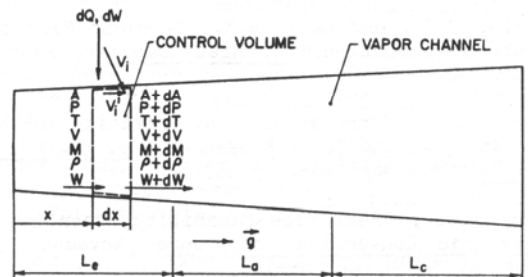
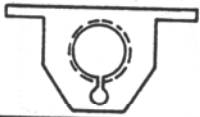

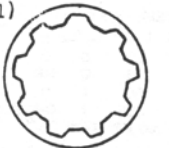
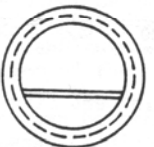
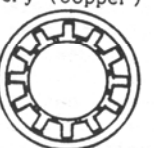



Fig. 5 Definition of the control volume and variables for the compressible vapor flow analysis

Table 1. High performance heat pipe concepts

Wick design	Performance Specification
<b>Monogroove</b> (Al extrusion) 	NH <sub>3</sub> tests: at 21°C $L_{eff} = 4.6m$ $D_v = 13.4mm, D_o = 6.32mm$ Slot gap width = 0.254mm $Q_i L_{eff} = 3,330 W\text{-m}$ (max. no tilt) $Q_r = 13.4 W/cm^2$ Developer: Grumman
<b>Tapered Artery</b> (Al extrusion) 	NH <sub>3</sub> tests: see table 2 also $L_{eff} = 5.45m$ $D_v = 12.2mm, D_o = 6.35mm$ Slot gap width = 0.254mm $Q_i L_{eff} = 5,200 W\text{-m}$ (max. no tilt) $Q_r = 9.5 W/cm^2$ Developer: Lockheed
<b>Trapezoidal Axially Grooved</b> (Al) 	NH <sub>3</sub> tests: 20-70°C $L_{eff} = 2.97m, D_o = 41mm, 32$ grooves Groove width: 0.13-0.8mm Groove depth: 4.0-4.4mm $Q_i L_{eff} = 11,000 W\text{-m}$ (3mm adv.tilt) $Q_r = 2.8 W/cm^2$ Developer: OAO Corporation
<b>Dual Slot</b> 	Methanol analysis: 120°C $L_{eff} = 4m, D = 25.4mm$ $Q_i L_{eff} = 18,800 W\text{-m}$ (max. no tilt) Stainless steel Developer: Grumman
<b>Double Wall Artery (Copper)</b> 	Water tests: 100°C $L_{eff} = 1.72m,$ $D_o = 22.2mm, D_i = 12.7mm$ $Q_i L_{eff} = 2,100 W\text{-m}$ (max. no tilt and 166°C) $Q_r = 16 W/cm^2$ Developer: Wright Aeronautical Laboratories
<b>Dual Pair Artery Liquid Metal</b> (Molybdenum alloy) 	Lithium tests: 1230°C $L_{eff} = 1.6m$ $D_o = 15.8mm, D_i = 14.2mm$ 1.5mm artery diameter 400 mesh screen $Q_i L_{eff} = 48,000 W\text{-m}$ $Q_r = 150 W/cm^2$ Developer: Los Alamos National Laboratory

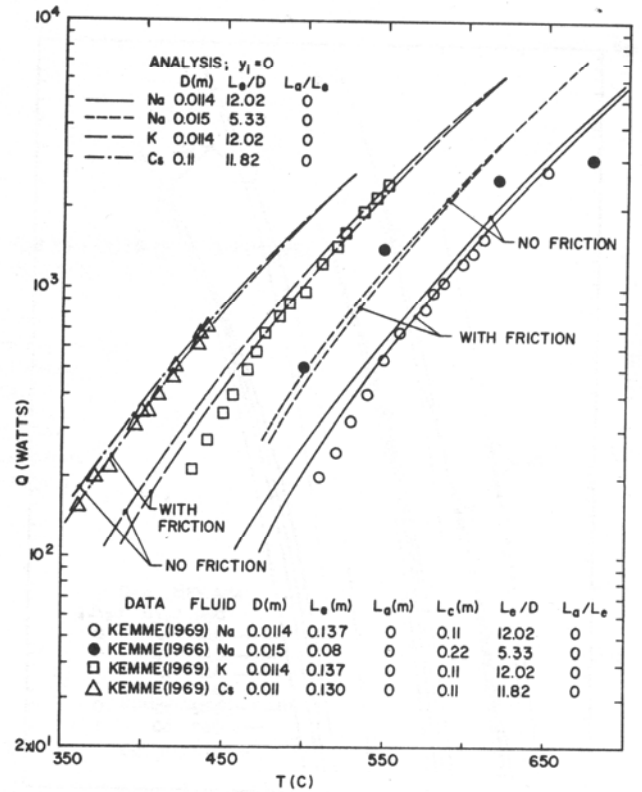


Fig. 6 Comparison of analytic results, with choking at the evaporator exit and with and without friction, with data

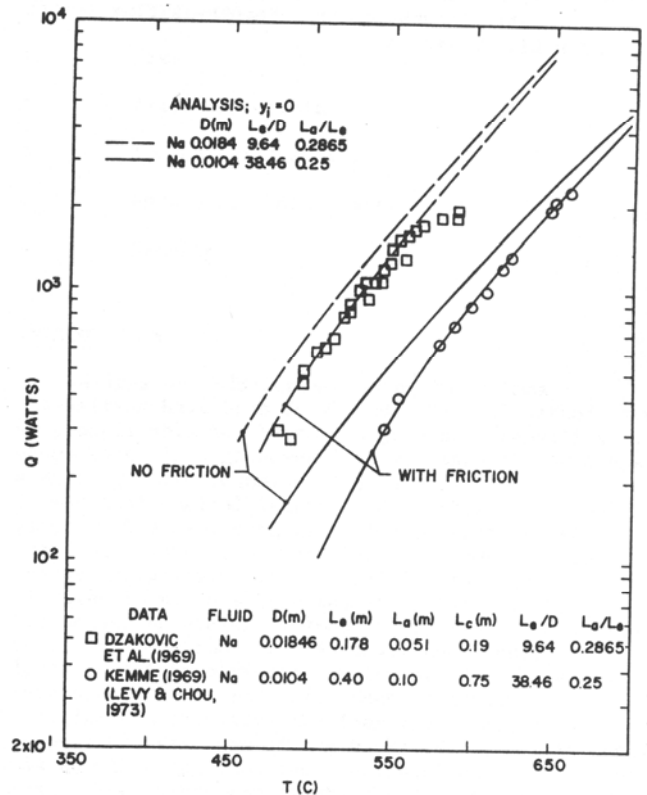


Fig. 7 Comparison of analytic results, with choking at the adiabatic section exit and with and without friction, with data

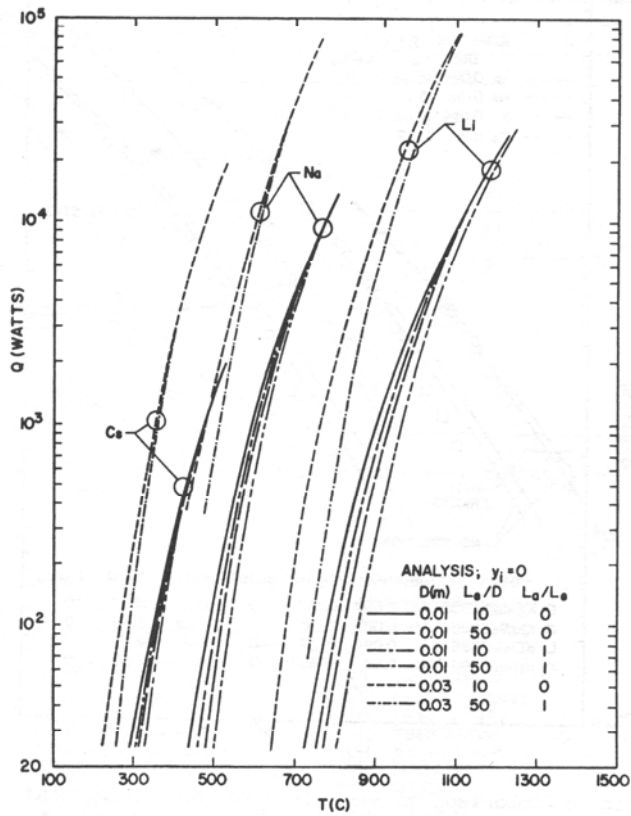


Fig. 8 The effect of vapor diameter, evaporator and adiabatic lengths on the sonic heat flux limits for Li, Na and Cs

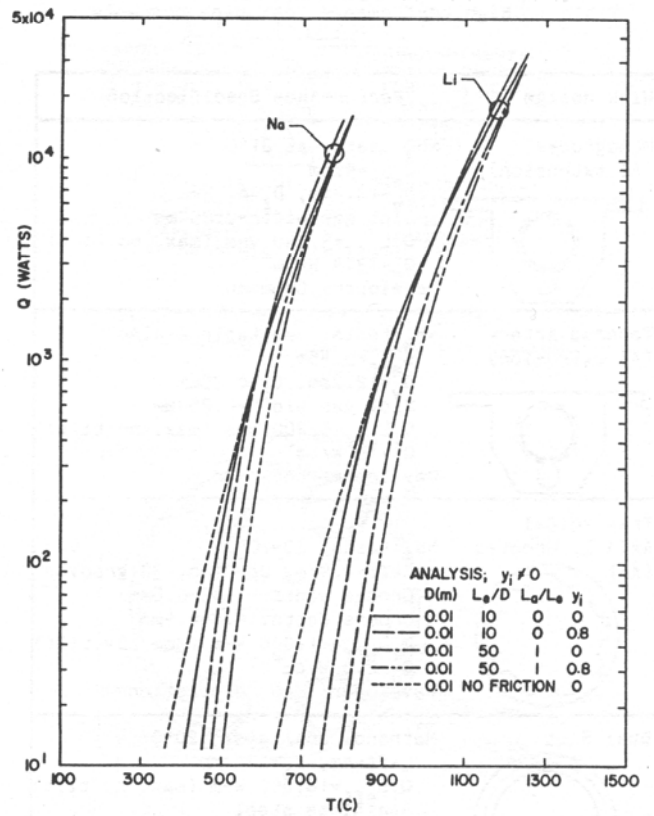


Fig. 9 The effect of  $y_i$  on the sonic heat flux limits for  $L_i$  and  $N_a$